Redefining Radar Perception for Autonomous Driving: The Role of Sparse Array and Waveform Design in 4D Automotive Radar

Shunqiao Sun[†] and Yimin D. Zhang[‡]

[†]The University of Alabama, Tuscaloosa, AL, USA

[‡]Temple University, Philadelphia, PA, USA

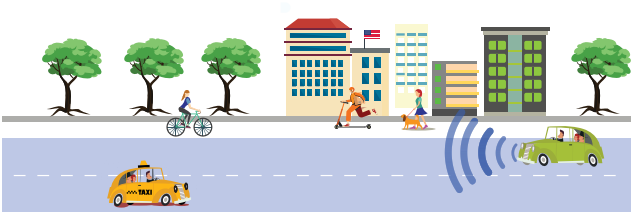

Supported in part by National Science Foundation (NSF) under Grants CCF-2153386 and ECCS-2236023

Outline

Imaging Radar for Fully Autonomous Driving

- Radar has emerged as one of the key technologies in autonomous driving systems.
  - Low-cost implementation
  - Resilient long-range sensing in all weather and lighting conditions
- MmWave automotive radar is required to offer high-resolution in 4D: range, Doppler, azimuth, and elevation[1]

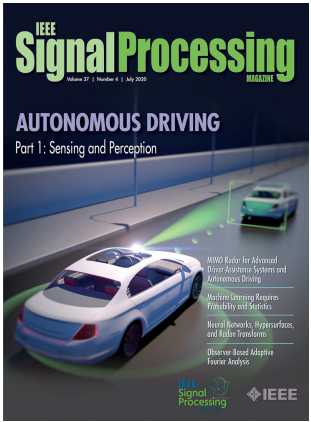

Technical challenges

- Large Aperture vs. Few Sensors
  - Sparse 2D array to achieve large aperture with few antennas
  - Ensure low-sidelobe sensing capability
- Robust Performance vs. Fast Response
  - DOA estimation under single snapshot
  - Difference coarray based on second-order statistics becomes challenging
- High Range/Doppler Resolution vs. Low Mutual Interference
  - Sparse orthogonal waveform design with low time and frequency occupancy
  - Sidelobe mitigation

Real-time 4D high-resolution imaging of diverse targets in the highly dynamic autonomous driving scenario using automotive radar with small form factor and low cost represents the hardest challenges.

[1] S. Sun, A. P. Petropulu, and H. V. Poor, "MIMO radar for advanced driver-assistance systems and autonomous driving: Advantages and challenges," *IEEE Signal Processing Magazine*, vol. 37, no. 4, pp. 98-117, 2020 (**Feature Article**).

Commercial 4D Imaging Radars in Early Stage

- Continental ARS540:
  - Long-range radar with maximum range of 300 meters
  - Azimuth FOV: [-60°, 60°]
  - Stepped frequency modulation
  - 12 TX and 16 RX, rendering 192 virtual array elements
  - Processor: Xilinx Zynq UltraScale+ MPSoC
- Aptiv FLR4+
  - Long-range radar with maximum range of 300 meters
  - 6TX and 8 RX, rendering 48 virtual array elements
- ZF Forward-Looking Full-Range Radar
  - Long-range radar with maximum range of 350 meters
  - Azimuth FOV: [-60°, 60°]
  - 12 TX and 16 RX, rendering 192 virtual array elements
- Other Startups:
  - Uhnder
  - Arbe Robotics
  - Aystx (now part of Cruise)
  - RadSee
  - Spartan Radar
  - Zadar Labs

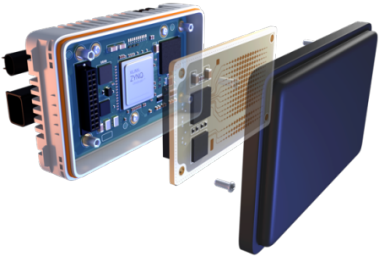

Source: Xilinx and Continental

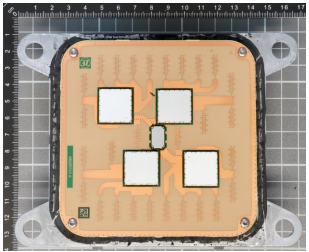

Source: FCC

High-Resolution Radar Low-Level Range-Azimuth Spectra in Bird's-Eye View

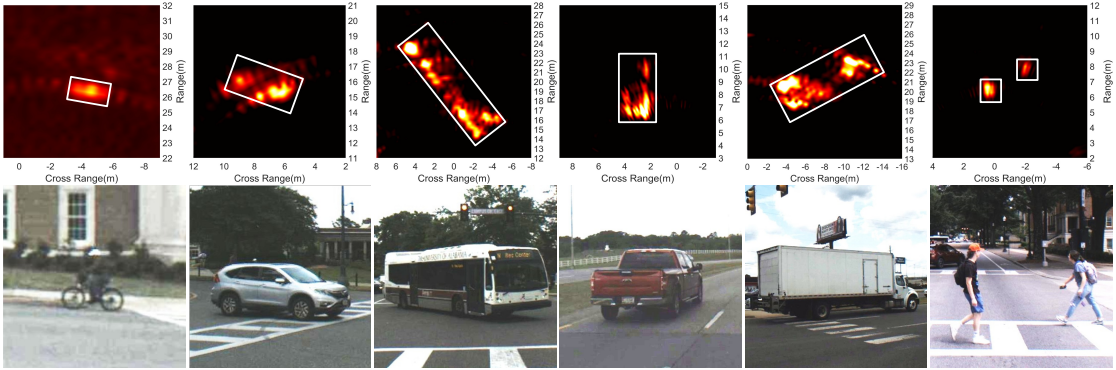

Figure 1: Zoom-in radar bird's-eye views of typical objects, such as bike, car, bus, truck, and pedestrian[2].

High-resolution radar low-level data representation (e.g., range-azimuth spectra) contains rich information of the object (e.g., shape) to support environmental perception for fully autonomous driving.

[2] R. Zheng, S. Sun, H. Liu and T. Wu, "Deep neural networks-enabled vehicle detection using high-resolution automotive radar imaging," *IEEE Transactions on Aerospace and Electronic Systems*, accepted for publication, 2023.

Importance of Information in Both Azimuth and Elevation Directions

- For autonomous driving, azimuth information alone does not ensure safe driving.
- Information in both azimuth and elevation is crucial [3].
  - The height information of targets is required to enable drive-over and drive-under functions.
  - It is safe to drive over a metal beverage can on the road and to drive under a steel pedestrian bridge over the road.
  - Without sufficient resolution in measuring elevation angles, automotive radars cannot make such decisions.
- To achieve a $\Delta\theta = 1^{\circ}$ resolution in both azimuth and elevation, a 2D array with an aperture of $D = 1.4/(\pi \sin(\Delta\theta/2)) \approx 51$ wavelengths is needed in each dimension.

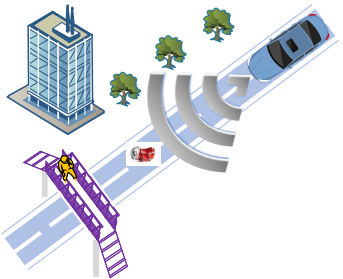

[3] S. Sun and Y. D. Zhang, "4D automotive radar sensing for autonomous vehicles: A sparsity-oriented approach," *IEEE Journal of Selected Topics in Signal Processing*, vol. 15, no. 4, pp. 879-891, 2021.

Sparsity in Angular Domain

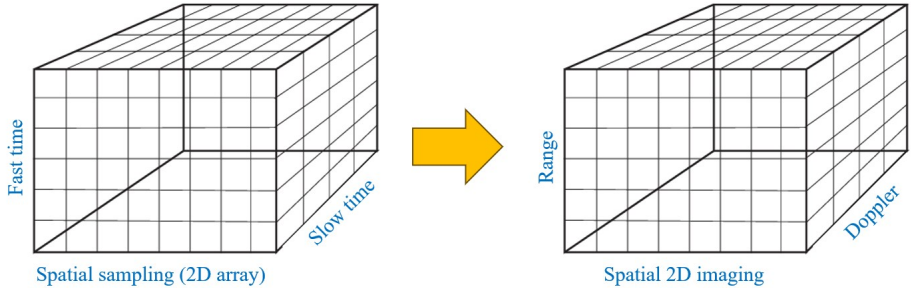

- Targets are first separated in range and Doppler domains.
- In the same range-Doppler bin, the number of targets that need to be resolved in the 2D spatial domain is small.
- Range-Doppler FFT operations yield significant SNR improvement (Raw data has extremely low SNR).
- One range-Doppler domain sample is treated as a snapshot for DOA estimation.

Sum Coarray Synthesis in MIMO Radar

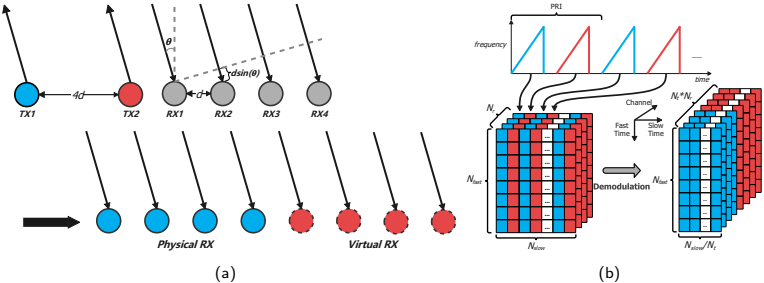

Figure 2: An example of MIMO radar with 8 virtual sum coarray elements, synthesized by 2 transmit and 4 receive antennas. (a) Physical and virtual arrays. (b) Illustration of waveform orthogonality through TDM.

- We first consider sum coarray and structured interpolation for linear arrays.
- In MIMO radar, sum coarray can be synthesized as $\mathbb{S} = \{x + y | x \in \mathbb{S}_T, y \in \mathbb{S}_R\}$, where $\mathbb{S}_T$ and $\mathbb{S}_R$ are TX and RX antenna positions.
- The waveforms transmitted from the transmit antennas are desired to be orthogonal. Waveform orthogonality may be achieved utilizing diversity in fast-time, slow-time, frequency, Doppler, and code domains.
- The example show time division multiplexing (TDM) in slow-time using frequency-modulated continuous-wave (FMCW). FMCW signals are commonly used because, after matched filtering, the target return signal becomes low-frequency complex sinusoids, known as *beat signal*, for convenient processing.

Hankel Matrix Completion for Sparse Linear Coarray

- The sum coarray may be designed to be sparse so as to achieve an desired aperture.
- When there are missing elements in the sum coarray, directly performing DOA estimation may yield high sidelobes and obstruct target detection.
- To reduce the sidelobe levels, missing elements in the "holes" need to be recovered through structured interpolation.
- For an M-element ULA, the noiseless array response $\mathbf{y} = [y_1, y_2, \cdots, y_M]^T$ can be used to construct a Hankel matrix with dimension $M_1 \times L$ as

$$\mathcal{H}(\mathbf{y}) = \begin{bmatrix} y_1 & y_2 & \cdots & y_L \\ y_2 & y_3 & \cdots & y_{L+1} \\ y_3 & y_4 & \cdots & y_{L+2} \\ \vdots & \vdots & \ddots & \vdots \\ y_{M_1} & y_{M_1+1} & \cdots & y_M \end{bmatrix}$$

where L is the pencil parameter and $M_1 = M - L + 1$.

- When K ($K < M_1$ and $K < L$) sources imping to the array, the Hankel matrix $\mathcal{H}(\mathbf{y})$ has a Vandermonde decomposition structure $\mathcal{H}(\mathbf{y}) = \mathbf{A}\mathbf{\Sigma}_s\mathbf{B}^T$ with rank K, where

$$\mathbf{A} = [\mathbf{a}(\theta_1), \cdots, \mathbf{a}(\theta_K)] \text{ with } \mathbf{a}(\theta_k) = \left[1, e^{j2\pi \frac{d\sin(\theta_k)}{\lambda}}, \cdots, e^{j2\pi \frac{(M_1-1)d\sin(\theta_k)}{\lambda}}\right]^T$$

$$\mathbf{B} = [\mathbf{b}(\theta_1), \cdots, \mathbf{b}(\theta_K)] \text{ with } \mathbf{b}(\theta_k) = \left[1, e^{j2\pi \frac{d\sin(\theta_k)}{\lambda}}, \cdots, e^{j2\pi \frac{(L-1)d\sin(\theta_k)}{\lambda}}\right]^T$$

$$\mathbf{\Sigma}_s = \text{diag}([\beta_1, \cdots, \beta_K])$$

Hankel Matrix Completion for Sparse Linear Coarray

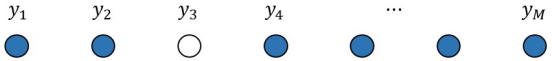

- Missing sum coarray elements render a Hankel matrix with missing elements:

$$\mathcal{H}(\mathbf{y}) = \begin{bmatrix} y_1 & y_2 & \cdots & y_L \\ y_2 & y_3 & \cdots & y_{L+1} \\ y_3 & y_4 & \cdots & y_{L+2} \\ \vdots & \vdots & \ddots & \vdots \\ y_{M_1} & y_{M_1+1} & \cdots & y_M \end{bmatrix}$$

- The forward-only Hankel matrix completion problem[4] is to find a Hankel matrix $\mathcal{H}(\mathbf{x})$ that has a minimum rank and its distance to the original data matrix at the observed positions meets the required error bound δ:

$$\min_{\mathbf{x}} \ \operatorname{rank}\left(\mathcal{H}(\mathbf{x})\right)$$
$$\text{s.t.} \ \ \left\|\mathcal{H}(\mathbf{x}) \odot \mathbf{M}_{FO} - \mathcal{H}(\mathbf{y})\right\|_F \leq \delta,$$

where $\mathbf{M}_{FO}$ is a mask matrix.

[4] S. Sun and Y. D. Zhang, "4D automotive radar sensing for autonomous vehicles: A sparsity-oriented approach," *IEEE Journal of Selected Topics in Signal Processing*, vol. 15, no. 4, pp. 879-891, 2021.

Forward-Backward Hankel Matrix Completion for One-Dimensional Sparse Array[5]

Theorem

The noiseless conjugate backward array response can be written as $\bar{\mathbf{y}} = \left[y_M^*, y_{M-1}^*, \cdots, y_1^*\right]^T$. *Formulate a block Hankel matrix* $\mathbf{Y}_{FB} = \left[\begin{array}{cc} \mathcal{H}(\mathbf{y}) & \mathcal{H}(\bar{\mathbf{y}}) \end{array}\right] \in \mathbb{C}^{M_1 \times 2L}$. *The rank of the forward-backward block Hankel matrix* $\mathbf{Y}_{FB} = [\mathcal{H}(\mathbf{y}) | \mathcal{H}(\bar{\mathbf{y}})] \in \mathbb{C}^{M_1 \times 2L}$ *is* K *if* $M_1 > K$ *and* $L > K/2$.

- In foward only case, $L = \left\lfloor \frac{M+1}{2} \right\rfloor$, and the FO data matrix has dimension of $\left\lfloor \frac{M+1}{2} \right\rfloor \times \left\lfloor \frac{M+1}{2} \right\rfloor$.
- In forward-backward case, $L = \left\lfloor \frac{M+1}{3} \right\rfloor$, and the FB data matrix has dimension of $2\left\lfloor \frac{M+1}{3} \right\rfloor \times 2\left\lfloor \frac{M+1}{3} \right\rfloor$. The FB data matrix has a larger dimension than the FO data matrix while having the same rank.
- The noisy matrix completion is formulated as a rank minimization problem, defined below

$$\begin{aligned} &\min_{\mathbf{x}} \ \operatorname{rank}\left(\left[\begin{array}{cc} \mathcal{H}(\mathbf{x}) & \mathcal{H}(\bar{\mathbf{x}}) \end{array}\right]\right) \\ &\text{s.t.} \ \left\| \left[\begin{array}{cc} \mathcal{H}(\mathbf{x}) & \mathcal{H}(\bar{\mathbf{x}}) \end{array}\right] \odot \mathbf{M}_{FB} - \mathbf{Z}_{FB}^S \right\|_F \leq \delta. \end{aligned}$$

[5] S. Sun, Y. Wen, R. Wu, D. Ren, and J. Li, "Fast forward-backward Hankel matrix completion for automotive radar DOA estimation using sparse linear arrays," *IEEE Radar Conference*, San Antonio, TX, May 2023.

Fast Forward-Backward Hankel Matrix Completion Using Iterative Hard Thresholding

- In the n-th iteration, the new forward-backward array beamvectors $\mathbf{X}_n = \begin{bmatrix} \mathbf{x}_n & \bar{\mathbf{x}}_n \end{bmatrix} \in \mathbb{C}^{M\times 2}$ is updated as

$$\mathbf{X}_n = \mathbf{X}_{n-1} - \alpha_n \mathbf{D}_{n-1},$$

where $\alpha_n = \frac{1}{\sqrt{n}}$ is the step size, and $\mathbf{D}_{n-1} \in \mathbb{C}^{M\times 2}$ is the sub-gradient, defined as

$$\mathbf{D}_{n-1} = \begin{bmatrix} \mathbf{z}_S & \bar{\mathbf{z}}_S \end{bmatrix} - \mathbf{X}_{n-1} \odot \begin{bmatrix} \mathbf{m} & \bar{\mathbf{m}} \end{bmatrix}.$$

- In the n-th iteration, the obtained FB Hankel matrix $\mathbf{H}_n = \begin{bmatrix} \mathcal{H}(\mathbf{x}_n) & \mathcal{H}(\bar{\mathbf{x}}_n) \end{bmatrix} = \mathbf{U}_n \mathbf{\Sigma}_k \mathbf{V}_n^H$, with $\mathbf{U}_n \in \mathbb{C}^{M_1\times K}$ and $\mathbf{V}_n \in \mathbb{C}^{2L\times K}$, is first projected onto a tangent subspace $\mathbf{T}_n \in \mathbb{C}^{M_1\times 2L}$, which is defined as

$$\mathbf{T}_n = \{\mathbf{U}_n \mathbf{A}^H + \mathbf{B}\mathbf{V}_n^H | \mathbf{A} \in \mathbb{C}^{2L\times K}, \mathbf{B} \in \mathbb{C}^{M_1\times K}\}.$$

- The projection can be rewritten as

$$\mathcal{P}_{\mathbf{T}_n}\mathbf{H}_n = \begin{bmatrix} \mathbf{U}_n & \mathbf{Q}_2 \end{bmatrix} \mathbf{M}_n \begin{bmatrix} \mathbf{V}_n & \mathbf{Q}_1 \end{bmatrix}^H,$$

where

$$\mathbf{M}_n = \begin{bmatrix} \mathbf{U}_n^H \mathbf{H}_n \mathbf{V}_n & \mathbf{R}_1^H \\ \mathbf{R}_2 & \mathbf{0} \end{bmatrix} \in \mathbb{C}^{2K\times 2K}.$$

Here, $\mathbf{Q}_1 \in \mathbb{C}^{2L\times K}$ and $\mathbf{R}_1 \in \mathbb{C}^{K\times K}$ are from QR decompositions of the following matrix of dimensional $2L \times K$, with computational cost of $\mathcal{O}\left(2LK^2\right)$.

$$\left(\mathbf{I} - \mathbf{V}_n \mathbf{V}_n^H\right) \mathbf{H}_n^H \mathbf{U}_n = \mathbf{Q}_1 \mathbf{R}_1,$$
$$\left(\mathbf{I} - \mathbf{U}_n \mathbf{U}_n^H\right) \mathbf{H}_n \mathbf{V}_n = \mathbf{Q}_2 \mathbf{R}_2.$$

Fast Forward-Backward Hankel Matrix Completion Using Iterative Hard Thresholding, Cont'd

- The multiplications of $\mathbf{H}_n^H \mathbf{U}_n$ and $\mathbf{H}_n \mathbf{V}_n$ can be computed efficiently via fast Fourier transform (FFT) with computational cost of $\mathcal{O}(KM \log M)$. Let the reverse of the k-th column of the matrix $\mathbf{V}_n$ be $\overleftarrow{\mathbf{v}}_k = \mathrm{rev}(\mathbf{v}_k) = \left[\overleftarrow{\mathbf{v}}_{1k}, \overleftarrow{\mathbf{v}}_{2k}\right]^T \in \mathbb{C}^{2L\times 1}$. The multiplication of FB Hankel matrix with a vector is computed efficiently via FFT[6]

$$\mathbf{f} = \mathrm{ifft}\left[\mathrm{fft}\left(\mathrm{vec}\left(\mathbf{X}_n\right)\right) \odot \mathrm{fft}\left(\hat{\mathbf{v}}_k\right)\right],$$

  where $\hat{\mathbf{v}}_k = \left[\overleftarrow{\mathbf{v}}_{1k}, \mathbf{0}, \overleftarrow{\mathbf{v}}_{2k}, \mathbf{0}\right]^T \in \mathbb{C}^{2M\times 1}$ is a zero-padding vector with $\mathbf{0}$ being a zero vector of length $M-L$. By extracting the last M_1 elements of $\mathbf{f}$, we have

$$\mathbf{H}_n \mathbf{v}_k = \mathrm{extract}\left(\mathbf{f}\right).$$

- FB Hankel matrix $\mathbf{H}_n$ is projected on to the set of rank K matrices.

$$\mathbf{H}_{n+1} = \mathcal{D}_K \mathcal{P}_{\mathbf{T}_n}\left[\begin{array}{cc} \mathcal{H}\left(\mathbf{x}_n\right) & \mathcal{H}\left(\bar{\mathbf{x}}_n\right) \end{array}\right]$$

  where the hard thresholding operator $\mathcal{D}_K$ computes the rank K approximation via truncated SVD.

[6] L. Lu, W. Xu, and S. Qiao, "A fast SVD for multilevel block Hankel matrices with minimal memory storage," *Numerical Algorithms*, vol. 69, pp. 875–891, 2015.

Fast Forward-Backward Hankel Matrix Completion Using Iterative Hard Thresholding, Cont'd

- The rank K truncated SVD of $\mathbf{M}_n \in \mathbb{C}^{2K\times 2K}$ can be represented as $\mathbf{M}_n = \mathbf{U}_M\mathbf{\Sigma}_M\mathbf{V}_M^H$ which can be computed in $\mathcal{O}\left(K^3\right)$ flops. Then the SVD of $\mathbf{H}_{n+1}$ can be written as

$$\mathbf{H}_{n+1} = \left(\underbrace{\begin{bmatrix}\mathbf{U}_n & \mathbf{Q}_2\end{bmatrix}\mathbf{U}_M}_{\mathbf{U}_{n+1}}\right)\underbrace{\mathbf{\Sigma}_M}_{\mathbf{\Sigma}_{n+1}}\left(\underbrace{\begin{bmatrix}\mathbf{V}_n & \mathbf{Q}_1\end{bmatrix}\mathbf{V}_M}_{\mathbf{V}_{n+1}}\right)^H$$

- Finally, update the estimate of $\mathbf{X}_{n+1} = \begin{bmatrix}\mathbf{x}_{n+1} & \bar{\mathbf{x}}_{n+1}\end{bmatrix}$ as

$$\mathbf{x}_{n+1} = \sum_{k=1}^{K}[\mathbf{\Sigma}_{n+1}]_{k,k}\mathcal{H}^+\left([\mathbf{U}_{n+1}]_{:,k}\left([\mathbf{V}_{n+1}]_{1:L,k}\right)^H\right)$$

$$\bar{\mathbf{x}}_{n+1} = \sum_{k=1}^{K}[\mathbf{\Sigma}_{n+1}]_{k,k}\mathcal{H}^+\left([\mathbf{U}_{n+1}]_{:,k}\left([\mathbf{V}_{n+1}]_{L+1:2L,k}\right)^H\right)$$

where $\mathcal{H}^+$ denotes the left inverse of $\mathcal{H}$, i.e.,

$$\left[\mathcal{H}^+\left([\mathbf{U}_{n+1}]_{:,k}\left([\mathbf{V}_{n+1}]_{1:L,k}\right)^H\right)\right]_t = \frac{1}{\rho_t}\sum_{a+b=t}[\mathbf{U}_{n+1}]_{a,k}[\mathbf{V}_{n+1}]^*_{b,k},$$

$$\left[\mathcal{H}^+\left([\mathbf{U}_{n+1}]_{:,k}\left([\mathbf{V}_{n+1}]_{L+1:2L,k}\right)^H\right)\right]_t = \frac{1}{\rho_t}\sum_{a+b=t}[\mathbf{U}_{n+1}]_{a,k}[\mathbf{V}_{n+1}]^*_{L+b,k},$$

where ρ_t denotes the number of entries on the t-th anti-diagonal of $\mathcal{H}\left(\mathbf{x}_{n+1}\right)$ or $\mathcal{H}\left(\bar{\mathbf{x}}_{n+1}\right)$. It can be computed efficiently via fast convolution with computational cost of $\mathcal{O}\left(KM\log M\right)$.

Fast Forward-Backward Hankel Matrix Completion

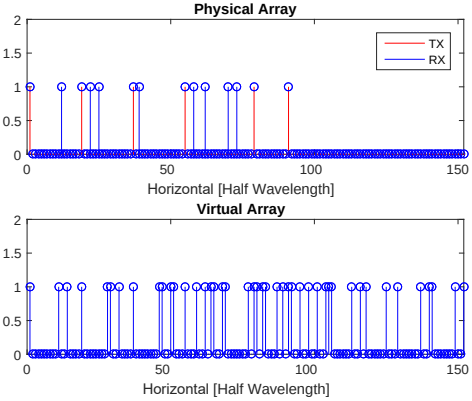

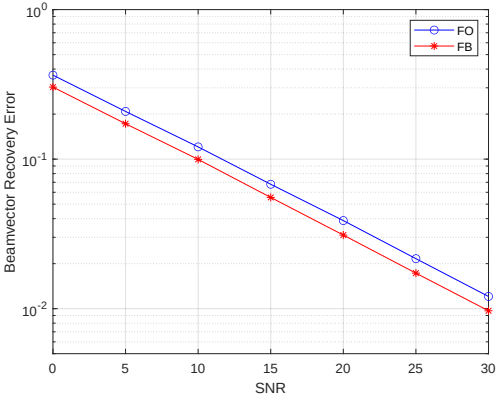

Figure 3: Example of beamvector recovery error for an automotive radar with virtual sparse array of 48 elements and aperture of 76λ.

- For the forward only case, the pencil parameter is chosen as $L = 76$ and the dimension of FO Hankel matrix is 76×76. For the FB case, the pencil parameter is chosen as $L = 51$ and the dimension of FB Hankel matrix is 102×102.

2D Sparse Array Completion

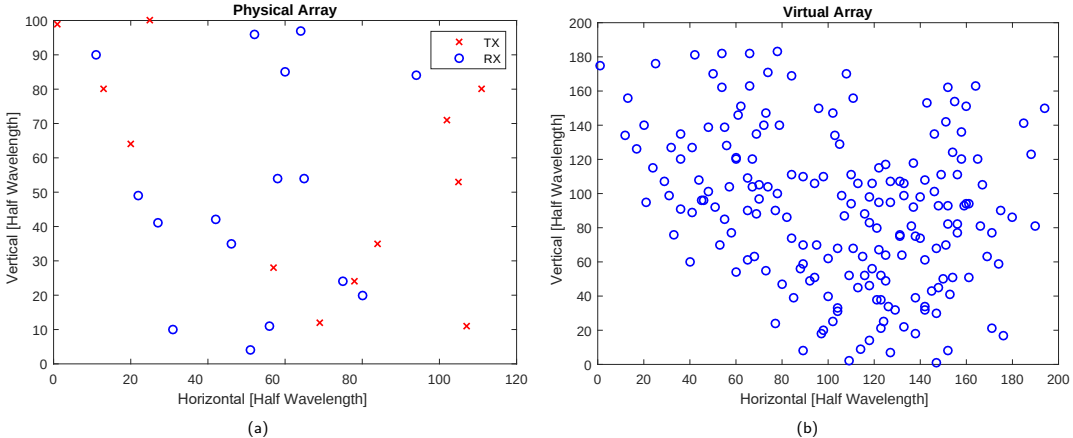

Figure 4: A MIMO radar with 12 transmit antennas and 16 receive antennas by cascading 4 automotive radar transceivers. The transmit and receive antennas are randomly deployed in an area of $[0, 100]\,(\lambda/2) \times [0, 120]\,(\lambda/2)$ to synthesize a MIMO 2D virtual array of 196 elements.

2D Sparse Array Completion

- We can construct an $N_1 \times (M_1 - N_1 + 1)$ block Hankel matrix as

$$\mathbf{Y}_E = \begin{bmatrix} \mathbf{Y}_0 & \mathbf{Y}_1 & \cdots & \mathbf{Y}_{M_1-N_1} \\ \mathbf{Y}_1 & \mathbf{Y}_2 & \cdots & \mathbf{Y}_{M_1-N_1+1} \\ \vdots & \vdots & \ddots & \vdots \\ \mathbf{Y}_{N_1-1} & \mathbf{Y}_{N_1} & \cdots & \mathbf{Y}_{M_1-1} \end{bmatrix},$$

  where

$$\mathbf{Y}_m = \begin{bmatrix} x_{m,0} & x_{m,1} & \cdots & x_{m,M_2-L} \\ x_{m,1} & x_{m,2} & \cdots & x_{m,M_2-L+1} \\ \vdots & \vdots & \ddots & \vdots \\ x_{m,L-1} & x_{m,L} & \cdots & x_{m,M_2-1} \end{bmatrix},$$

  is an $L \times (M_2 - L + 1)$ Hankel matrix, and $x_{m_1,m_2} = \sum_{k=1}^{K} \beta_k e^{j\pi((m_1-1)\sin(\chi_k)+(m_2-1)\sin(\varphi_k))}$.

- The noisy block Hankel matrix completion problem is formulated as[7]:

$$\min \ \|\mathbf{X}_E\|_* \quad \text{s.t.} \quad \|\mathcal{P}_\Omega(\mathbf{X} - \mathbf{M}^o)\|_{\mathrm{F}} \leq \delta.$$

[7] S. Sun and Y. D. Zhang, "4D automotive radar sensing for autonomous vehicles: A sparsity-oriented approach," *IEEE Journal of Selected Topics in Signal Processing*, vol. 15, no. 4, pp. 879-891, 2021.

2D Sparse Array Completion

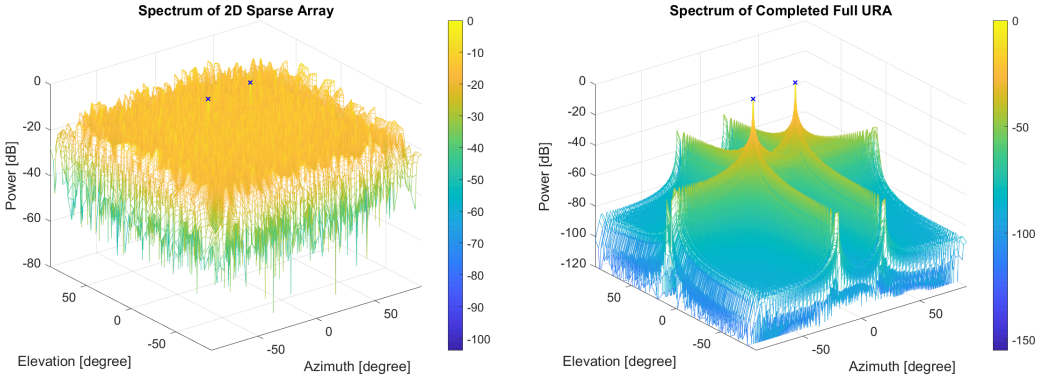

(a) (b)

Figure 5: The spectrum of two targets with azimuth and elevation angles of $(\chi_1, \varphi_1) = (-20^\circ, 5^\circ), (\chi_2, \varphi_2) = (20^\circ, 10^\circ)$ under the sparse array. The targets' angles are marked with crosses. (a) There are high sidelobes in the spectrum due to the existing of large number of holes in the sparse array. (b) Sidelobe is suppressed in the competed array.

Identifiability of Hankel Matrix: Coherence[8]

Let $\mathbf{U}$ and $\mathbf{V}$ be left and right subspaces of the singular value decomposition of Hankel matrix $\mathbf{Y} \in \mathbb{C}^{N\times N}$, which has rank K. The coherence of $\mathbf{U}$ (similarly for $\mathbf{V}$) equals

$$\mu(U) = \frac{N}{K} \max_{1\le i\le N} \|\mathbf{U}(i,:)\|^2 \in \left[1, \frac{N}{K}\right].$$

Matrix $\mathbf{Y}$ has coherence with parameters μ_0 and μ_1 if

- (B1) $\max(\mu(U), \mu(V)) \le \mu_0$ holds for some positive μ_0.
- (B2) The maximum element of matrix $\sum_{1\le i\le K} \mathbf{u}_i \mathbf{v}_i^H$ is upper bounded by $\mu_1\sqrt{K}/N$ in absolute value for some positive μ_1.

Theorem

(Coherence of Hankel Matrix $\mathbf{Y}$): Consider the Hankel matrix $\mathbf{Y}$ constructed from a uniform linear array and assume that the set of target angles $\{\theta_k\}_{k\in\mathbb{N}_K^+}$ consists of almost surely distinct members, with minimal spatial frequency separation

$x = \min_{(i,j)\in\mathbb{N}_K^+\times\mathbb{N}_K^+, i\neq j} \frac{d}{\lambda}(\sin\theta_i - \sin\theta_j)$ *satisfying* $|x| \ge \xi \neq 0$. *If* $K \le \sqrt{\frac{N}{\beta_N(\xi)}}$ *where* $\beta_N(\xi) = \frac{1}{N}\frac{\sin^2(\pi N\xi)}{\sin^2(\pi\xi)}$ *is the Fejér kernel, the matrix* $\mathbf{Y}$ *satisfies the conditions (B1) and (B2) with coherence parameters* $\mu_0 \triangleq \frac{\sqrt{N}}{\sqrt{N}-(K-1)\sqrt{\beta_N(\xi)}}$ *and* $\mu_1 \triangleq \mu_0\sqrt{K}$ *with probability* 1.

When entries of matrix $\mathbf{Y}$ are observed uniformly at random, there are constants C and c such that if

$$m \ge C \max\left(\mu_1^2, \mu_0^{1/2}\mu_1, \mu_0 N^{1/4}\right) \zeta K N \log N$$

holds for some $\zeta > 2$, the minimizer to the nuclear norm optimization is unique and equals to $\mathbf{Y}$ with probability of $1 - cN^{-\zeta}$.

[8] S. Sun and Y. D. Zhang, "4D automotive radar sensing for autonomous vehicles: A sparsity-oriented approach," *IEEE Journal of Selected Topics in Signal Processing*, vol. 15, no. 4, pp. 879-891, 2021.

Identifiability of Hankel Matrix: Sparse Array Topology

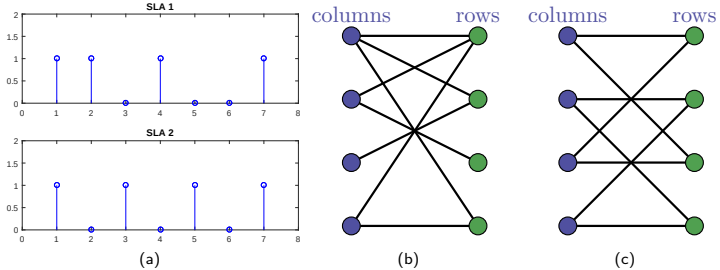

Figure 6: Examples of SLAs: (a) two SLAs and the corresponding bipartite graphs (b) $\mathcal{G}_1$ and (c) $\mathcal{G}_2$.

For the above two different SLAs, the Hankel matrices with missing elements are

$$\mathbf{Y}_1 = \begin{bmatrix} 1 & \gamma & * & \gamma^3 \\ \gamma & * & \gamma^3 & * \\ * & \gamma^3 & * & * \\ \gamma^3 & * & * & \gamma^6 \end{bmatrix}, \ \mathbf{Y}_2 = \begin{bmatrix} 1 & * & \gamma^2 & * \\ * & \gamma^2 & * & \gamma^4 \\ \gamma^2 & * & \gamma^4 & * \\ * & \gamma^4 & * & \gamma^6 \end{bmatrix}.$$

Let $\mathcal{G} = (V, E)$ be a bipartite graph associated with the sampling operator $\mathcal{P}_\Omega$, where $V = \{1, 2, \cdots, N\} \cup \{1, 2, \cdots, N\}$ and $(i, j) \in E$ iff $(i, j) \in \Omega$. Let $\mathbf{G} \in \mathbb{R}^{N \times N}$ be the biadjacency matrix of the bipartite graph $\mathcal{G}$ with $\mathbf{G}_{ij} = 1$ iff $(i, j) \in \Omega$. It can be seen that $\mathcal{G}_1$ is connected, while $\mathcal{G}_2$ is not.

Identifiability of Hankel Matrix: Sparse Array Topology

- Necessary condition: connectivity of the bipartite graph associated with the sampling operator $\mathcal{P}_\Omega$ is a necessary condition for matrix completion.

- Sufficient conditions of matrix completion involve the matrix coherence properties and the spectral gap of the graph $\mathcal{G}$, which is defined as the difference $\sigma_1(\mathbf{G}) - \sigma_2(\mathbf{G})$ between the largest singular value $\sigma_1(\mathbf{G})$ and the second largest singular value $\sigma_2(\mathbf{G})$ of $\mathbf{G}$ [9].

- If the spectral gap of matrix $\mathbf{G}$ is sufficiently large, the nuclear norm minimization method exactly recovers the low-rank matrix satisfying the coherence condition. It can be verified that $\mathcal{G}_2$ depicted in Fig. 6(c) is a 2-regular graph with vertex connectivity $\sigma_1(\mathbf{G}) = \sigma_2(\mathbf{G}) = 2$. Thus the spectral gap of $\mathbf{G}_2$ is zero and $\mathbf{Y}$ cannot be recovered from $\mathbf{Y}_2$.

- The spectra gap condition provides a guidance for choosing the location of sparse array elements. The sparse arrays can be optimized such that the bipartite graph associated with the sampling operator $\mathcal{P}_\Omega$, i.e., the locations of virtual array elements, has a large spectra gap.

[9] S. Bhojanapalli and P. Jain, "Universal matrix completion," *International Conference on Machine Learning*, Beijing, China, pp. 1881-1889, June 2014.

High-Resolution DOA Estimation with Single Snapshot

- The array response can be written as

$$\mathbf{y} = \mathbf{A}(\boldsymbol{\theta})\mathbf{s} + \mathbf{n},$$

where $\mathbf{A}(\boldsymbol{\theta}) = [\mathbf{a}(\theta_1), \mathbf{a}(\theta_2), \cdots, \mathbf{a}(\theta_K)]$ is $N \times K$ array manifold matrix with $\mathbf{a}(\theta) = \left[1, e^{\frac{2\pi d_2}{\lambda}\sin\theta}, \cdots, e^{\frac{2\pi d_N}{\lambda}\sin\theta}\right]^T$, and $\mathbf{n}$ denotes a spatially white noise term.

- For single-snapshot case, $\mathbf{y}\mathbf{y}^H$ is rank-one, so subspace-based DOA estimation methods cannot be directly applied.

Similarity to Difference Coarray Domain Formulation

- In multi-snapshot DOA estimation problems with

$$\mathbf{y}(t) = \mathbf{A}(\boldsymbol{\theta})\mathbf{s}(t) + \mathbf{n}(t),$$

the covariance matrix is computed as

$$\mathbf{R} = E[\mathbf{y}(t)\mathbf{y}^H(t)] = \mathbf{A}(\theta)\mathbf{R_s}\mathbf{A^H}(\theta) + \sigma_{\mathbf{n}}^{\mathbf{2}}\mathbf{I}$$

- Vectorizing $\mathbf{R}$ yields

$$\mathrm{vec}(\mathbf{R}) = \tilde{\mathbf{A}}(\theta)\mathrm{vec}(\mathbf{R_s}) + \sigma_{\mathbf{n}}^{\mathbf{2}}\mathrm{vec}(\mathbf{I})$$

where $\tilde{\mathbf{A}}(\theta)$ is the Khatri–Rao product between $\mathbf{A}^*(\theta)$ and $\mathbf{A}(\theta)$.

- This rank-one DOA estimation problem is well considered in sparse array design utilizing difference coarray.

Subspace-based DOA Estimation Methods

- When the array data is complete or completed, spatial smoothing of rank-one $\mathbf{y}\mathbf{y}^H$ can restore the rank so subspace-based DOA estimation can be applied. [10] [11]
- Alternatively, single-snapshot MUSIC can be implemented through the SVD of $\mathcal{H}(\mathbf{y})$ [12]:

$$\mathcal{H}(\mathbf{y}) = \begin{bmatrix} y_1 & y_2 & \cdots & y_L \\ y_2 & y_3 & \cdots & y_{L+1} \\ y_3 & y_4 & \cdots & y_{L+2} \\ \vdots & \vdots & \ddots & \vdots \\ y_{M_1} & y_{M_1+1} & \cdots & y_M \end{bmatrix} = \mathbf{U}\mathbf{\Sigma}\mathbf{V}^T,$$

with $\mathbf{U} = [\mathbf{U}_s \;\; \mathbf{U}_n]$ and $\mathbf{V} = [\mathbf{V}_s \;\; \mathbf{V}_n]$ dividing them into signal and noise subspaces.

- The MUSIC spectrum can be computed as $J(\theta) = \frac{||\mathbf{a}(\theta)||_2^2}{||\mathbf{U}_n^H\mathbf{a}(\theta)||_2^2}$, where $\mathbf{a}(\theta)$ is the steering vector corresponding to DOA θ.

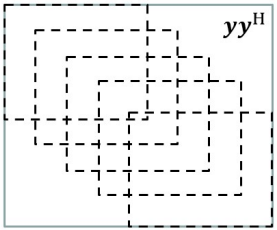

[10] T.-J. Shan, M. Wax, and T. Kailath, "On spatial smoothing for direction-of-arrival estimation of coherent signals," *IEEE Transactions on Acoustics, Speech, and Signal Processing*, vol. 33, no. 4, pp. 806–811, Aug. 1985.

[11] P. Pal and P. P. Vaidyanathan, "Coprime sampling and the MUSIC algorithm," *IEEE Digital Signal Processing Workshop and IEEE Signal Processing Education Workshop*, Sedona, AZ, Jan. 2011.

[12] W. Liao and A. Fannjiang, "MUSIC for single-snapshot spectral estimation: Stability and super-resolution," *Applied and Computational Harmonic Analysis*, vol. 40, pp. 33–67, 2016.

Compressive Sensing-based DOA Estimation

- Compressive sensing methods can solve rank-one problem and do not require the array data to be consecutive. [13].
- For example, the solution can be formulated as a LASSO expression to find sparse solutions of $\hat{\mathbf{s}}$ [14] [15] :

$$\hat{\mathbf{s}} = \arg\min_{\mathbf{x}} \ ||\mathbf{x}||_1 \ \text{ subject to } \ ||\mathbf{y} - \mathbf{A}(\Omega)\mathbf{x}||_2 < \epsilon$$

  where $\mathbf{A}(\Omega)$ is the dictionary manifold matrix of the array defined over a dense angular grid and ϵ is a user-specific error bound.
- At a higher complexity, sparse Bayesian learning approach may provide higher sparse reconstruction ability and is more flexible to incorporate side information. [16]
- By modeling $\mathbf{x} \sim \mathcal{CN}(\mathbf{0}, \mathrm{diag}(\boldsymbol{\alpha}))$ and $\mathbf{n} \sim \mathcal{CN}(\mathbf{0}, \beta\mathbf{I})$, sparse Bayesian learning method maximizes the posterior probability

$$\Pr(\mathbf{x}|\mathbf{y}, \mathbf{A}(\Omega), \boldsymbol{\alpha}, \beta)$$

  where $\boldsymbol{\alpha}$ and β are determined by maximizing their marginal likelihood.

[13] S. Qin, Y. D. Zhang, and M. G. Amin, "Generalized coprime array configurations for direction-of-arrival estimation," *IEEE Transactions on Signal Processing*, vol. 63, no. 6, pp. 1377–1390, March 2015.

[14] Y. D. Zhang, M. G. Amin, and B. Himed, "Sparsity-based DOA estimation using co-prime arrays," *IEEE International Conference on Acoustics, Speech, and Signal Processing*, Vancouver, Canada, May 2013.

[15] S. Fortunati, R. Grasso, F. Gini and M. S. Greco, "Single snapshot DOA estimation using compressed sensing," *IEEE International Conference on Acoustics, Speech and Signal Processing (ICASSP)*, Florence, Italy, 2014.

[16] Q. Wu, Y. D. Zhang, M. G. Amin, and B. Himed, "Complex multitask Bayesian compressive sensing," *IEEE International Conference on Acoustics, Speech, and Signal Processing*, Florence, Italy, May 2014.

DOA Estimation for Spatially Continuous Targets

- For targets with spatial continuity, sparse Bayesian learning can take the spatial dependency of targets into account, thereby providing enhanced accuracy than subspace-based methods, such as MUSIC.
- To encourage the group sparsity with neighboring entries, a spike-and-slab prior on $\mathbf{x}$ can be placed as [17]

$$\Pr(\mathbf{x}|\boldsymbol{\pi},\beta) = \prod_{i=1}^{|\mathbf{x}|}[(1-\pi_i)\delta(r_i) + \pi_i \mathcal{CN}(r_i|0,\beta)]$$

where $\boldsymbol{\pi} = [\pi_1, \cdots, \pi_G]^T$ determines the probability of the nonzero elements of $\mathbf{x}$.

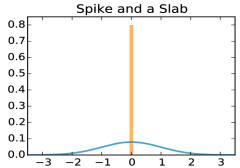

- The value of π_i of each entry can be adjusted based on the neighboring entries, rendering "strong rejection", "weak rejection", and "strong acceptance" for the three cases illustrated below.
- Such approach provides close solutions for continuous target, whereas MUSIC spectra tend to only emphasize edges.

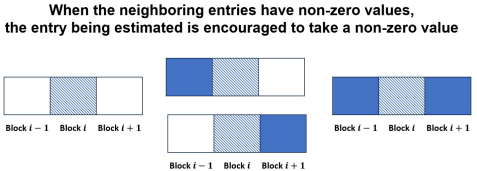

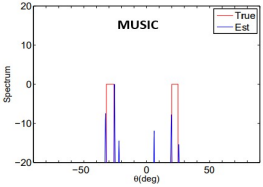

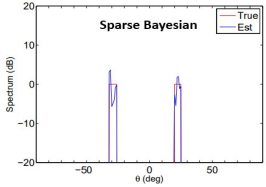

[17] S. Qin, Y. D. Zhang, Q. Wu, and M. G. Amin, "DOA estimation of nonparametric spreading spatial spectrum based on Bayesian compressive sensing exploiting intra-task dependency," *IEEE International Conference on Acoustics, Speech, and Signal Processing*, Brisbane, Australia, April 2015.

Single-Snapshot DOA Estimation Using Machine Learning Methods

- Data-driven deep learning (DL) for DOA estimation typically model it as a multi-label classification task for on-grid angles.
- DL-based DOA estimation achieves fast inference time, enhanced super-resolution capabilities, and better performance at low SNR [18].
- By considering imperfect channel conditions and array calibration errors in the training phase, DL-based DOA estimation can be made more robust to these factors [19].
- Data-driven DL approach requires a large amount of data to train the network and lacks generalization and interpretability.
- For iterative optimization problems, algorithm unrolling replaces the iteration steps of optimization algorithm with recurrent neural network layers [20].

[18] G. K. Papageorgiou, M. Sellathurai and Y. C. Eldar, "Deep networks for direction-of-arrival estimation in low SNR," *IEEE Transactions on Signal Processing*, vol. 69, pp. 3714-3729, 2021.

[19] M. S. R. Pavel, M. W. T. S. Chowdhury, Y. D. Zhang, D. Shen, and G. Chen, "Machine learning-based direction-of-arrival estimation exploiting distributed sparse arrays," *Asilomar Conference on Signals, Systems, and Computers*, Pacific Grove, CA, Oct. 2021.

[20] V. Monga, Y. Li and Y. C. Eldar, "Algorithm Unrolling: Interpretable, Efficient deep learning for signal and image processing," *IEEE Signal Processing Magazine*, vol. 38, no. 2, pp. 18-44, March 2021.

Iterative Adaptive Approach (IAA) Algorithm

- Iterative Adaptive Approach (IAA) [21] [22] minimizes the weighted least-square $(\mathbf{y} - s_l\mathbf{a}(\theta_l))^H\mathbf{Q}^{-1}(\theta_l)(\mathbf{y} - s_l\mathbf{a}(\theta_l))$, where $\mathbf{Q}(\theta_l) = \mathbf{R} - P_l\mathbf{a}(\theta_l)\mathbf{a}^H(\theta_l)$ is the interference covariance matrix. The solution is $\hat{s}_l = \frac{\mathbf{a}^H(\theta_l)\mathbf{R}^{-1}\mathbf{y}}{\mathbf{a}^H(\theta_l)\mathbf{R}^{-1}\mathbf{a}(\theta_l)}$.
- Iteration: For P discretized angles, IAA iteratively computes $\mathbf{R} = \sum_{l=1}^{P} |\hat{s}_l|^2\mathbf{a}^H(\theta_l)\,\mathbf{a}(\theta_l)$ and $\hat{s}_l = \frac{\mathbf{a}^H(\theta_l)\mathbf{R}^{-1}\mathbf{y}}{\mathbf{a}^H(\theta_l)\mathbf{R}^{-1}\mathbf{a}(\theta_l)}$ until converge.

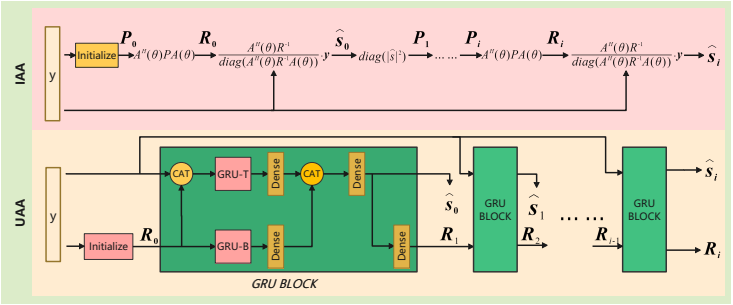

[21] W. Roberts, P. Stoica, J. Li, T. Yardibi and F. A. Sadjadi, "Iterative Adaptive Approaches to MIMO Radar Imaging," *IEEE Journal of Selected Topics in Signal Processing*, vol. 4, no. 1, pp. 5–20, Feb. 2010.

[22] T. Yardibi, J. Li, P. Stoica, M. Xue and A. B. Baggeroer, "Source Localization and Sensing: A Nonparametric Iterative Adaptive Approach Based on Weighted Least Squares," *IEEE Transactions on Aerospace and Electronic Systems*, vol. 46, no. 1, pp. 425-443, Jan. 2010.

Unrolling Iteration Adaptive Approach (UAA) Networks

Unrolling iterative adaptive approach (UAA) [23] unrolls the IAA algorithm into multiple deep neural network layers that avoids the high computational costs associated with matrix inversions.

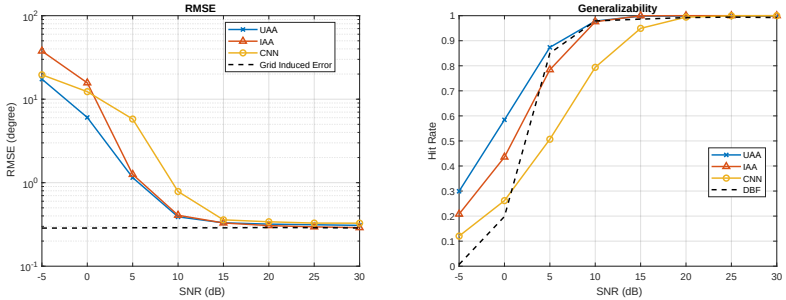

Figure 7: RMSE of estimated DOA of a single, randomly generated off-grid target versus input SNR.

- 20-element ULA with inter-element spacing of half-wavelength to generate beam vectors for maximal 3 targets with a minimum separation of $\Delta\phi = 6°$.
- For each Monte Carlo trial, an off-grid source with a direction randomly drawn from interval $[-30°, 30°]$ is generated.

[23] R. Zheng, H. Liu, S. Sun, and J. Li, "Deep learning based computationally efficient unrolling IAA for direction-of-arrival estimation," *European Signal Processing Conference (EUSIPCO)*, Helsinki, Finland, Sept. 2023.

1. Overview of High-Resolution Imaging Radar for Autonomous Driving
2. 2D Sparse Array: Achieving Large Aperture with Few Sensors
3. Single-Snapshot DOA Estimation: Achieving Fast Response with Robust Performance
4. Sparse Waveform Design: Achieving High Range/Doppler Resolution with Low Mutual Interference

Sparse Step-Frequency MIMO Radar Design for Autonomous Driving

- State-of-the-art automotive radar systems exploit FMCW signals at millimeter-wave frequencies.
- To achieve a high range resolution for autonomous driving, the transmit signals are designed to occupy a large bandwidth.
- For conventional automotive FMCW radars, the frequency linearly sweeps over the entire bandwidth, thereby making the signal susceptible to interference from other automotive radars.
- The sparse step-frequency waveform (SSFW) radar transmits several pulses within a large bandwidth, where some frequencies are unused during a CPI.
- An SSFW radar can avoid or reduce multiuser interference by skipping the spectrum bands that are occupied by other radars.
- Consider a sequence of N pulses whose carrier frequencies are a sparse subset chosen from P available frequencies, $\mathcal{M} = \{f_n | f_c + n\Delta f, n \in \{0, 1, \cdots, P-1\}\}$, that are equally distributed in $[f_c, f_c + B]$. The maximum unambiguous range is $R_u = c/(2\Delta f)$ whereas the range resolution is given by $\Delta R = c/(2P\Delta f) = R_u/P$.

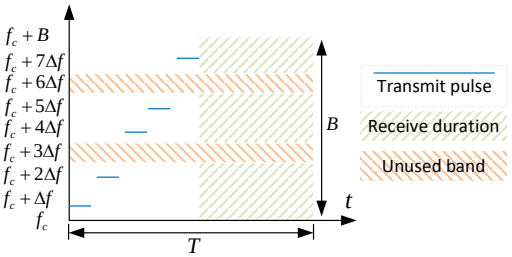

Sparse Step-Frequency MIMO Radar Design for Autonomous Driving

- The transmit antenna transmits a sequence of N pulses whose carrier frequencies are sparsely distributed over the available bandwidth of B. The carrier frequencies $f_n \in [f_c, f_c + B]$, $n = 1, 2, \cdots, N$, are randomly chosen from the set $\mathcal{M} = \{f_n | f_c + h_n \Delta f, h_n \in \{1, 2, \cdots, P\}\}$ with $P = \lfloor B/\Delta f \rfloor$ equally spaced subcarriers.
- The range and Doppler are estimated via IDFT over fast time samples and FFT over slow-time samples, respectively.
- Since the carrier frequencies are uniformly divided and randomly chosen, the range spectrum would have high sidelobes. As a result, targets with a small RCS may be obscured by the range sidelobes of stronger targets.
- We introduce a joint two-phase optimization technique to achieve desirable range sidelobe level[24]. The sparse carrier frequencies among the set $f_n \in [f_c, f_c + B]$ are first optimally selected using the the particle swarm optimization (PSO) technique such that the peak sidelobe level (PSL) of the range spectrum is minimized.
- We then introduce a complex weight vector to further minimize the range spectrum PSL[25].
- The IDFT of the weighted fast-time samples can be written as $F_m(l) = \frac{1}{P} \sum_{n=0}^{P-1} w_n y(m, n) e^{j2\pi \frac{l}{P} n}$.
- In the frequency domain, the obtained range spectrum will be the convolution of frequency response of sparse weights $\mathbf{w}$ and frequency response of the original range data $\mathbf{y}_m$. Therefore, the spectrum of the sparse weights $\mathbf{w}$ is desired to have low sidelobe levels over the entire sidelobe region so that the possible high range sidelobes in the resulting convolution would be minimized.

[24] S. Sun, L. Xu and N. S. Jeong, "Sparse step-frequency MIMO radar design for autonomous driving," *IEEE Radar Conference*, Atlanta, GA, May 2021.

[25] S. Sun and Y. D. Zhang, "4D automotive radar sensing for autonomous vehicles: A sparsity-oriented approach," *IEEE Journal of Selected Topics in Signal Processing*, vol. 15, no. 4, pp. 879-891, 2021.

Sparse Step-Frequency MIMO Radar Design for Autonomous Driving

- We discretize the entire unambiguous range R_u into a fine grid of Q points, r_q, $q = 1, \cdots, Q$, separated by ΔR, and set $r_f = R_u/2$ as the range corresponding to mainlobe. The sidelobe area is then described by set $\mathcal{Q} = \{r_1, \cdots, r_f - \Delta R, r_f + \Delta R, \cdots, R_u\}$. Define a range steering vector with respect to range r_q as $\mathbf{b}(r_q) = [b_1(r_q), \cdots, b_P(r_q)]^T$, where

$$b_n(r_q) = \begin{cases} e^{-j2\pi \frac{2r_q}{c} f_n}, & \text{if} \quad f_n \in \mathcal{M}, \\ 0, & \text{if } f_n \notin \mathcal{M}. \end{cases}$$

- The power spectrum of the ranges corresponding to sidelobe in $\mathcal{Q}$ is constrained to be below a threshold η determined by peak sidelobe level (PSL), i.e., $\eta = 10^{V_{\max}/10}$, where $V_{\max}$ is the maximum allowed PSL in dB. The weight optimization can be viewed as a range sidelobe minimization problem and is formulated as

$$\begin{aligned} \min_{\mathbf{w},\alpha} \ & \alpha \\ \text{s.t.} \quad & \left|\mathbf{w}^H \mathbf{b}(r_q)\right| \le \eta + \alpha, \quad r_q \in \mathcal{Q}, \\ & \mathbf{w}^H \mathbf{b}(r_f) = 1 \end{aligned}$$

- The above optimization problem is convex and can be solved efficiently.
- Waveform orthogonality for SSFW: All transmit antennas simultaneously transmit the RSSFW waveform at the same sparse carrier frequencies. We adopt phase coding in slow time to achieve waveform orthogonality via Doppler division multiplexing (DDM)[26]. Each pulse has the same phase code in one burst cycle, and the phase code varies with different burst pulse cycles.

[26] S. Sun, A. P. Petropulu, and H. V. Poor, "MIMO radar for advanced driver-assistance systems and autonomous driving: Advantages and challenges," *IEEE Signal Processing Magazine*, vol. 37, no. 4, pp. 98-117, 2020 (**Feature Article**).

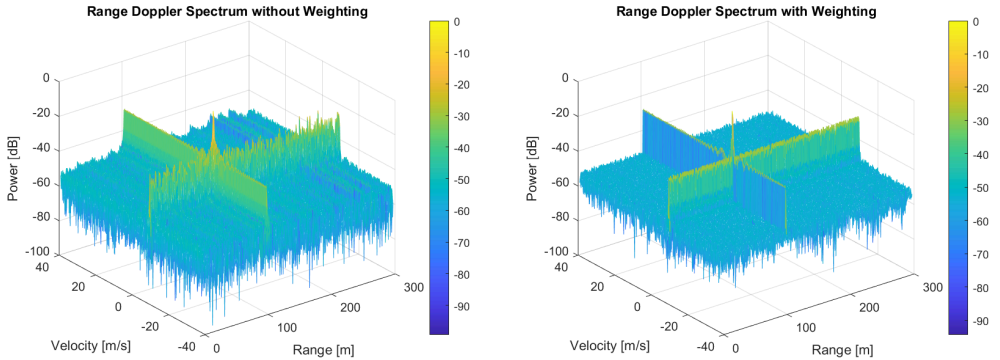

Figure 8: Illustration of range and Doppler spectrum for two targets with equal power located at range of 100 m with velocity of -10 m/s. (a) spectra without weighting; (b) spectra with weighting.

Sparse Step-Frequency MIMO Radar Design for Autonomous Driving

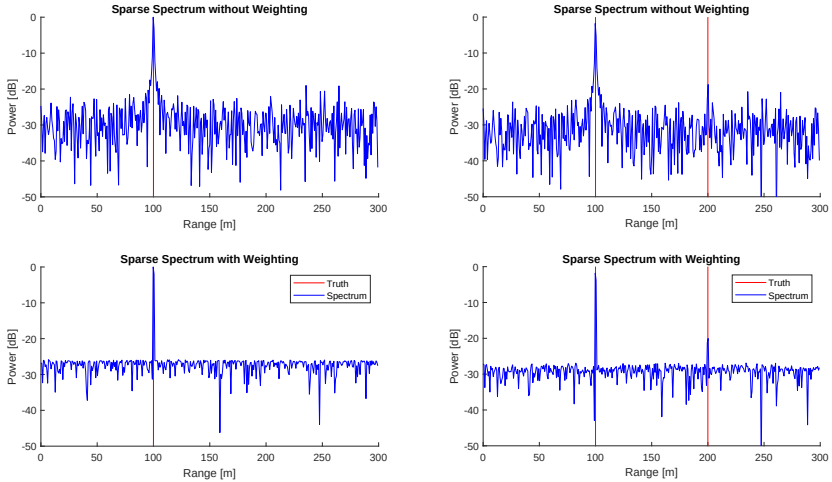

Figure 9: Comparison of range spectrum with and without weighting. (a) Two targets with equal power located at the same range of $R = 100$ m. (b) Two targets are located at different ranges of 100 m and 200 m with normalized power of 1 and 0.1, respectively.

Concluding Remarks

- **Radar provides reliable 4D imaging solutions for autonomous driving**
  - Much lower cost compared to Lidar but achieves comparable resolution
  - Operational in all weather and lighting conditions
- **Sparse 2D array and waveform designs provide viable solutions to achieve high imaging resolution**
  - Extremely sparse 2D array to achieve the required aperture under the cost constraint
  - Sparse time and frequency occupancy supports multi-radar operations with low interference
- **Sophisticated signal processing methods become critical for 4D imaging and target detection**
  - Missing samples in space, time, and frequency inevitably cause high level of sidelobes obstructing target detection
  - Fast time-varying environment requires single- or few-snapshot 4D imaging
  - Data completion, CS, and ML methods and their combinations can be exploited
- **Significant challenges remain for future research and development**
  - Optimum design of extremely sparse 2D arrays that fit into practical requirements
  - High-resolution imaging in the presence of clutter and spatially clustered targets
  - More effective utilization of time and frequency resources for 4D imaging
  - Low-complexity signal processing methods with reliability and robustness

References

Automotive Radar

- S. Sun, A. P. Petropulu and H. V. Poor, "MIMO radar for advanced driver-assistance systems and autonomous driving: Advantages and challenges," *IEEE Signal Processing Magazine*, vol. 37, no. 4, pp. 98-117, 2020. (Feature Article)
- S. Sun and Y. D. Zhang, "4D automotive radar sensing for autonomous vehicles: A sparsity-oriented approach," *IEEE Journal of Selected Topics in Signal Processing*, vol. 15, no. 4, pp. 879-891, 2021.
- S. Sun and Y. D. Zhang, "Four-dimensional high-resolution automotive radar imaging exploiting joint sparse-frequency and sparse-array design," *IEEE 46th Intl. Conf. on Acoustics, Speech, and Signal Processing (ICASSP)*, Toronto, Canada, June 2021.
- R. Zheng, S. Sun, D. Scharff and T. Wu, "SpectraNet: A High resolution imaging radar deep neural network for autonomous vehicles," *IEEE Sensor Array and Multichannel Signal Processing Workshop (SAM)*, Trondheim, Norway, June 2022.
- L. Xu, R. Zheng, and S. Sun, "A deep reinforcement learning approach for integrated automotive radar sensing and communication," *IEEE Sensor Array and Multichannel Signal Processing Workshop (SAM)*, Trondheim, Norway, June 2022.
- R. Zheng, S. Sun, H. Liu and T. Wu, "Deep neural networks-enabled vehicle detection using high-resolution automotive radar imaging," *IEEE Transactions on Aerospace and Electronic Systems*, in press, 2023.

Sparse Array and DOA Estimation

- Y. D. Zhang, M. G. Amin, and B. Himed, "Sparsity-based DOA estimation using co-prime arrays," *IEEE International Conference on Acoustics, Speech, and Signal Processing*, Vancouver, Canada, May 2013.
- S. Qin, Y. D. Zhang, Q. Wu, and M. G. Amin, "DOA estimation of nonparametric spreading spatial spectrum based on Bayesian compressive sensing exploiting intra-task dependency," *IEEE International Conference on Acoustics, Speech, and Signal Processing*, Brisbane, Australia, April 2015.
- A. Hassanien, M. G. Amin, Y. D. Zhang, and F. Ahmad, "High-resolution single-snapshot DOA estimation in MIMO radar with colocated antennas," *IEEE International Radar Conference*, Arlington, VA, May 2015.
- S. Sun and A. P. Petropulu, "A sparse linear array approach in automotive radars using matrix completion," *IEEE 45th International Conference on Acoustics, Speech, and Signal Processing (ICASSP)*, Barcelona, Spain, May 2020.
- S. Zhang, A. Ahmed, Y. D. Zhang, and S. Sun, "DOA estimation exploiting interpolated multi-frequency sparse array," *IEEE Sensor Array and Multichannel Signal Processing Workshop (SAM)*, Hangzhou, China, June 2020. (Best Student Paper Award)
- S. Sun and Y. D. Zhang, "Multi-frequency sparse array-based massive MIMO radar for autonomous driving," *54th Annual Asilomar Conference on Signals, Systems, and Computers (Asilomar)*, Pacific Grove, CA, Nov. 2020.
- S. Zhang, A. Ahmed, Y. D. Zhang and S. Sun, "Enhanced DOA estimation exploiting multi-frequency sparse array," *IEEE Transactions on Signal Processing*, vol. 69, pp. 5935-5946, 2021.

References (Cont'd)

Sparse Array and DOA Estimation (Cont'd)

- A. Ahmed and Y. D. Zhang, "Generalized non-redundant sparse array designs," *IEEE Transactions on Signal Processing*, vol. 69, pp. 4580-4594, Aug. 2021.
- L. Xu and S. Sun, "Coprime visible regions assisted angle unfolding for sparse ESPRIT," *IEEE Radar Conference*, San Antonio, TX, May 2023.
- S. Sun, Y. Wen, R. Wu, D. Ren, and J. Li, "Fast forward-backward Hankel matrix completion for automotive radar DOA estimation using sparse linear arrays," *IEEE Radar Conference*, San Antonio, TX, May 2023.
- L. Xu, S. Sun, Y. D. Zhang and A. P. Petropulu, "Joint antenna selection and beamforming in integrated automotive radar sensing-communications with quantized double phase shifters," *IEEE International Conference on Acoustics, Speech, and Signal Processing (ICASSP)*, Rhodes Island, Greece, June 2023.
- S. Sun and C. Li, "$1 + 1$ is greater than 2: Collaborative automotive radar imaging exploiting spatial diversity," *European Radar Conference (EuRAD)*, Berlin, Germany, Sept. 2023.
- R. Zheng, H. Liu, S. Sun, and J. Li, "Deep learning based computationally efficient unrolling IAA for direction-of-arrival estimation," *European Signal Processing Conference (EUSIPCO)*, Helsinki, Finland, Sept. 2023.
- R. Zheng, S. Sun, W. Kuo, T. Abatzoglou, and M. Markel, "4D automotive radar exploiting sparse array optimization and compressive sensing," *Asilomar Conference on Signals, Systems, and Computers (Asilomar)*, Pacific Grove, CA, Oct. 2023.
- L. Xu, S. Sun, R. Wu, D. Ren, and J. Li, "Generalized optimization of sparse antenna arrays for high-resolution automotive radar imaging," *Asilomar Conference on Signals, Systems, and Computers (Asilomar)*, Pacific Grove, CA, Oct. 2023.

Waveform Design and Range/Doppler Estimation

- X. Zhao, A. P. Petropulu and S. Sun, "A joint design of MIMO-OFDM dual-function radar communication system using generalized spatial modulation," *IEEE Radar Conference*, Florence, Italy, Sept. 2020.
- S. Sun, L. Xu and N. S. Jeong, "Sparse step-frequency MIMO radar design for autonomous driving," *IEEE Radar Conference*, Atlanta, GA, May 2021.
- L. Xu, S. Sun and K. V. Mishra, "Difference co-chirps-based non-uniform PRF automotive FMCW radar," *IEEE International Conference on Autonomous Systems (ICAS)*, Montréal, Québec, Canada, Aug 2021.
- R. Zheng, H. Liu, and S. Sun, "A deep learning approach for Doppler unfolding in automotive TDM MIMO radar," *Asilomar Conference on Signals, Systems, and Computers (Asilomar)*, Pacific Grove, CA, Oct. 2022.
- L. Xu, S. Sun, K. V. Mishra and Y. D. Zhang, "Automotive FMCW radar with difference co-chirps," *IEEE Transactions on Aerospace and Electronic Systems*, in press, 2023.
- R. Zheng, S. Sun, H. Liu, and T. Wu, "Time-sensitive and distance-tolerant deep learning-based vehicle detection using high-resolution radar birds-eye-view images," *IEEE Radar Conference*, San Antonio, TX, May 2023.

Thank You!

https://ssun.people.ua.edu
http://yiminzhang.com

LISC @ UA houses a 2021 Lexus RX450 Hybrid SUV as vehicle platform for autonomous driving, mounted with multimodal sensors (Velodyne LiDAR, mmWave Radars, FLIR Blackfly S Stereo Cameras, Novatel PwrPak7D RTK GPS/GNSS and Epson G370N IMU) and rack-mounted computers.